

HIGH ORDER LOCAL DISCONTINUOUS GALERKIN METHODS FOR THE ALLEN-CAHN EQUATION: ANALYSIS AND SIMULATION*

Ruihan Guo

*School of Mathematical Sciences, University of Science and Technology of China, Hefei,
Anhui 230026, P.R. China.*

Email: guoguo88@mail.ustc.edu.cn.

Liangyue Ji

Department of Mathematics, University of Minnesota-twin cities, Minneapolis, MN 55455 USA.

Email: jil@math.umn.edu.

Yan Xu¹⁾

*School of Mathematical Sciences, University of Science and Technology of China, Hefei,
Anhui 230026, P.R. China.*

Email: yxu@ustc.edu.cn.

Abstract

In this paper, we present a local discontinuous Galerkin (LDG) method for the Allen-Cahn equation. We prove the energy stability, analyze the optimal convergence rate of $k + 1$ in L^2 norm and present the $(2k + 1)$ -th order negative-norm estimate of the semi-discrete LDG method for the Allen-Cahn equation with smooth solution. To relax the severe time step restriction of explicit time marching methods, we construct a first order semi-implicit scheme based on the convex splitting principle of the discrete Allen-Cahn energy and prove the corresponding unconditional energy stability. To achieve high order temporal accuracy, we employ the semi-implicit spectral deferred correction (SDC) method. Combining with the unconditionally stable convex splitting scheme, the SDC method can be high order accurate and stable in our numerical tests. To enhance the efficiency of the proposed methods, the multigrid solver is adapted to solve the resulting nonlinear algebraic systems. Numerical studies are presented to confirm that we can achieve optimal accuracy of $\mathcal{O}(h^{k+1})$ in L^2 norm and improve the LDG solution from $\mathcal{O}(h^{k+1})$ to $\mathcal{O}(h^{2k+1})$ with the accuracy enhancement post-processing technique.

Mathematics subject classification: 65M60, 35K55, 35L02

Key words: Local discontinuous Galerkin method, Allen-Cahn equation, Energy stability, Convex splitting, Spectral deferred correction, A priori error estimate, Negative norm error estimate.

1. Introduction

In this paper, we develop a local discontinuous Galerkin (LDG) method and consider error estimates of the LDG method for the Allen-Cahn equation

$$u_t - \Delta u + \frac{1}{\varepsilon^2} f(u) = 0, \quad (1.1)$$

* Received July 11, 2014 / Revised version received June 19, 2015 / Accepted October 21, 2015 /
Published online March 6, 2016 /

¹⁾ Corresponding author

with the initial condition

$$u(\mathbf{x}, 0) = u_0(\mathbf{x}) \quad (1.2)$$

in a bounded domain with dimension $d \leq 3$. We assume that periodic boundary conditions are given. It is well-known that the Allen-Cahn equation is a gradient flow with the Liapunov energy functional

$$\mathcal{J}_\varepsilon(u) = \int_\Omega \Phi_\varepsilon(u) d\mathbf{x}, \quad \Phi_\varepsilon(u) = \frac{1}{2} |\nabla u|^2 + \frac{1}{\varepsilon^2} F(u), \quad (1.3)$$

where $F(u)$ is always positive and $f(u) = F'(u)$. A typical form of $F(u)$ is

$$F(u) = \frac{1}{4}(u^2 - 1)^2, \quad f(u) = u^3 - u. \quad (1.4)$$

As in [25], we shall impose a constraint on the potential function $F(u)$ by requiring $f(u)$ to satisfy

$$\max_{u \text{ solves Allen-Cahn}} |f'(u)| \leq L, \quad (1.5)$$

where L is a positive constant.

The Allen-Cahn equation (1.1) was originally introduced by Allen and Cahn [1] to describe the motion of anti-phase boundaries in crystalline solids. The function u represents the concentration of one of the two metallic components of the alloy and the positive parameter ε is called the diffuse interface width parameter. Recently, it has been applied to a wide range of problems such as the motion by mean curvature flows [14] and crystal growth [26]. In particular, it has become a basic model equation for the diffuse interface approach developed to study phase transitions and interfacial dynamics in materials science [5].

Various numerical methods have been developed to solve the Allen-Cahn equation. We refer the readers to [6, 7] for finite difference method. Feng *et al.* [15] developed an a posteriori error estimate for finite element approximations of the Allen-Cahn equation. Quasi-optimal a posteriori error estimates in $L^\infty(0, T; L^2(\Omega))$ was derived for finite element approximation in [2]. The numerical approximations of the celebrated Allen-Cahn equation and related diffuse interface models were studied in [34]. Yang [33] introduced a stabilized semi-implicit (in time) scheme and a splitting scheme for the equation. Feng *et al.* [13] recently presented the analysis for the fully discrete interior penalty discontinuous Galerkin (IP-DG) methods for the Allen-Cahn equation. In [16], the first- and second-order implicit-explicit schemes with parameters for solving the Allen-Cahn equation were investigated. Feng, Tang and Yang [17] combined the semi-implicit spectral deferred correction (SDC) method with energy stable convex splitting technique to solve a series of phase field models.

In this paper, we present an LDG method for the Allen-Cahn equation and prove its energy stability, where the energy is defined in (1.3). In addition, the optimal priori error estimate is also proved in L^2 norm for the LDG scheme. By employing a technical dual argument, we obtain an a priori error estimate in the negative-order norm for smooth solutions of Allen-Cahn equation, which is $2k + 1$, higher than the $(k + 1)$ -th order in L^2 -norm, where k ($k \geq 1$) is the highest degree polynomial used in the approximation. This negative norm error estimate is very essential for the accuracy enhancement post-processing technique [19, 20]. Additionally, we present numerical studies which confirm that we can achieve optimal accuracy of $\mathcal{O}(h^{k+1})$ in L^2 norm and improve the LDG solution from $\mathcal{O}(h^{k+1})$ to $\mathcal{O}(h^{2k+1})$ with the accuracy enhancement post-processing technique.

Numerical simulations of the Allen-Cahn equation, using explicit methods, will impose a severe time step restriction. To relax the severe time step restriction, we develop a semi-implicit temporal scheme which is based on the convex splitting technique of the discrete Allen-Cahn energy. The unconditional energy stability of the scheme is also proved. The scheme is stable regardless of time step size, unfortunately, it is first order accurate in time. To achieve high order temporal accuracy, the semi-implicit spectral deferred correction (SDC) method is adopted in this paper. The semi-implicit method will result in large system of algebraic equations at each time step and the efficiency of the semi-implicit method highly depends on the efficiency of the nonlinear solver. Traditional iterative methods such as Gauss-Seidel method suffers from slow convergence rates, especially for large system. To enhance the efficiency of the proposed approach, the nonlinear Full Approximation Storage (FAS) multigrid solver is employed to solve the resulting nonlinear system at each time step.

The discontinuous Galerkin (DG) method we discuss in this paper was first designed as a method for solving hyperbolic conservation laws containing only first order spatial derivatives, *e.g.* Reed and Hill [24] for solving linear transport equation. The LDG method is an extension of the DG method aimed at solving partial differential equations (PDEs) containing higher than first order spatial derivatives. The first LDG method was introduced by Cockburn and Shu [9] for time-dependent convection-diffusion systems. The idea of the LDG method is to rewrite the equations with higher order derivatives as a first order system, then apply the DG method to the system. The LDG methods have been developed for convection diffusion equations (containing second derivatives) [9], nonlinear one-dimensional and two-dimensional KdV type equations [30, 32] and Cahn-Hilliard equations [27, 29]. For a detailed description about the LDG methods for high-order time-dependent PDEs, we refer readers to the review paper [31].

The organization of the paper is as follows. In Section 2, we present an LDG method for the Allen-Cahn equation and prove the corresponding energy stability. We also design a semi-implicit convex splitting scheme which is first order accurate in time and prove the unconditional discrete energy stability. In Section 3, we prove an a priori error estimate in L^2 norm and the negative-order norm estimates of the LDG scheme for the Allen-Cahn equation. These results are confirmed numerically in Section 4. Finally, we give concluding remarks in Section 5.

2. The LDG Method and Semi-Implicit Time Marching Method for the Allen-Cahn Equation

2.1. Tessellation and function spaces

Let \mathcal{T}_h denote a tessellation of Ω with shape-regular elements K . Let Γ denote the union of the boundary faces of elements $K \in \mathcal{T}_h$, *i.e.* $\Gamma = \cup_{K \in \mathcal{T}_h} \partial K$. In order to describe the flux functions we need to introduce some notations. Let e be a face shared by the “left” and “right” elements K_L and K_R . For our purpose, “left” and “right” can be uniquely defined for each face according to any fixed rule, see, *e.g.* [31, 32] for more details of such a definition. Define the normal vectors ν_L and ν_R on e pointing exterior to K_L and K_R , respectively. If ψ is a function on K_L and K_R , but possibly discontinuous across e , let ψ_L denote $(\psi|_{K_L})|_e$ and ψ_R denote $(\psi|_{K_R})|_e$, the left and right trace, respectively.

Let $\mathcal{Q}^k(K)$ be the space of tensor product of polynomials of degree at most $k \geq 0$ on $K \in \mathcal{T}_h$

in each variable. The finite element spaces are denoted by

$$V_h = \left\{ \varphi \in L^2(\Omega) : \varphi|_K \in \mathcal{Q}^k(K), \quad \forall K \in \mathcal{T}_h \right\},$$

$$\Sigma_h = \left\{ \boldsymbol{\eta} = (\eta_1, \dots, \eta_d)^T \in (L^2(\Omega))^d : \eta_l|_K \in \mathcal{Q}^k(K), \quad l = 1 \dots d, \quad \forall K \in \mathcal{T}_h \right\}.$$

For one-dimensional case, we have $\mathcal{Q}^k(K) = \mathcal{P}^k(K)$, which is the space of polynomials of degree at most $k \geq 0$ defined on K . Note that functions in V_h and Σ_h are allowed to be completely discontinuous across element interfaces.

Here we only consider periodic boundary conditions. Notice that the assumption of periodic boundary conditions is for simplicity only and not essential: the method can be easily designed for non-periodic boundary conditions. The development of the LDG method for non-periodic boundary conditions can be found in [22].

Further, we define the inner product notations as

$$(w, v)_K = \int_K wvdK, \quad \langle w, v \rangle_{\partial K} = \int_{\partial K} wvds, \quad (2.1)$$

$$(\mathbf{q}, \mathbf{p})_K = \int_K \mathbf{q} \cdot \mathbf{p}dK, \quad \langle \mathbf{q}, \mathbf{p} \rangle_{\partial K} = \int_{\partial K} \mathbf{q} \cdot \mathbf{p}ds, \quad (2.2)$$

for scalar variables w, v and vector variables \mathbf{q}, \mathbf{p} respectively. The inner products on Ω are defined as

$$(w, v)_\Omega = \sum_K (w, v)_K, \quad (\mathbf{q}, \mathbf{p})_\Omega = \sum_K (\mathbf{q}, \mathbf{p})_K. \quad (2.3)$$

The definition we use below for the L^2 norm, L^∞ norm on the domain Ω and the boundary Γ are given by the standard definitions:

$$\|\eta\|_\Omega = \sqrt{(\eta, \eta)_\Omega}, \quad \|\eta\|_{L^\infty(\Omega)} = \text{esssup}_{x \in \Omega} |\eta|, \quad \|\eta\|_\Gamma = \sqrt{(\eta, \eta)_\Gamma}. \quad (2.4)$$

The l -norm in Ω is defined as

$$\|\eta\|_{l, \Omega} = \left(\sum_{|\alpha| \leq l} \|D^\alpha \eta\|_\Omega^2 \right)^{\frac{1}{2}}, \quad l > 0. \quad (2.5)$$

The negative-order norm is defined as: Given $l > 0$ and domain Ω ,

$$\|\eta\|_{-l, \Omega} = \sup_{\Phi \in C_0^\infty(\Omega)} \frac{(\eta, \Phi)_\Omega}{\|\Phi\|_{l, \Omega}}. \quad (2.6)$$

2.2. The LDG methods

In this section, we propose an LDG method for our model problem (1.1). First we rewrite Eq. (1.1) as a first-order system

$$u_t - \nabla \cdot \mathbf{q} + \frac{1}{\varepsilon^2} f(u) = 0, \quad (2.7a)$$

$$\mathbf{q} - \nabla u = 0. \quad (2.7b)$$

The approximations $(u_h, \mathbf{q}_h) \in (V_h, \Sigma_h)$ now can be defined as the solution of the following weak form

$$((u_h)_t, \psi)_K + (\mathbf{q}_h, \nabla \psi)_K - \langle \hat{\mathbf{q}}_h \cdot \boldsymbol{\nu}, \psi \rangle_{\partial K} + \frac{1}{\varepsilon^2} (f(u_h), \psi)_K = 0, \quad (2.8a)$$

$$(\mathbf{q}_h, \boldsymbol{\eta})_K + (u_h, \nabla \cdot \boldsymbol{\eta})_K - \langle \hat{u}_h, \boldsymbol{\eta} \cdot \boldsymbol{\nu} \rangle_{\partial K} = 0, \quad (2.8b)$$

with unknown approximation (u_h, \mathbf{q}_h) for all test functions $(\psi, \boldsymbol{\eta})$ from finite element space defined in Section 2.1. All the “hat” terms are numerical fluxes which are designed to guarantee stability of the LDG scheme. Here alternative flux is chosen

$$\hat{\mathbf{q}}_h|_e = \mathbf{q}_{h,R}, \quad \hat{u}_h|_e = u_{h,L}, \quad (2.9)$$

or

$$\hat{\mathbf{q}}_h|_e = \mathbf{q}_{h,L}, \quad \hat{u}_h|_e = u_{h,R}. \quad (2.10)$$

In this paper, (2.9) is used for the proof of the energy stability and the main error estimates.

2.3. Energy stability

It is shown by Feng and Prohl [14] that the Liapunov energy of Allen-Cahn equation decays with respect to time t , *i.e.* $\frac{d}{dt} \mathcal{J}_\varepsilon(u) \leq 0$. For LDG solution defined by scheme (2.8), it is possible to obtain the following similar energy stability.

Proposition 2.1. *The solution to the LDG scheme (2.8) with numerical fluxes (2.9) satisfies the energy stability*

$$\left(\frac{1}{2} (\mathbf{q}_h, \mathbf{q}_h)_\Omega + \frac{1}{\varepsilon^2} (F(u_h), 1)_\Omega \right) (t) \leq \left(\frac{1}{2} (\mathbf{q}_h, \mathbf{q}_h)_\Omega + \frac{1}{\varepsilon^2} (F(u_h), 1)_\Omega \right) (0), \quad (2.11)$$

$$\begin{aligned} & \left((u_h, u_h)_\Omega + \frac{1}{2} (\mathbf{q}_h, \mathbf{q}_h)_\Omega + \frac{1}{\varepsilon^2} (F(u_h), 1)_\Omega \right) (t) \\ & \leq e^{2t} \left((u_h, u_h)_\Omega + \frac{1}{2} (\mathbf{q}_h, \mathbf{q}_h)_\Omega + \frac{1}{\varepsilon^2} (F(u_h), 1)_\Omega \right) (0). \end{aligned} \quad (2.12)$$

Proof. Taking the time derivative of Eq. (2.8b), and choosing test functions $\psi = (u_h)_t$ and $\boldsymbol{\eta} = \mathbf{q}_h$, we obtain

$$((u_h)_t, (u_h)_t)_K + (\mathbf{q}_h, \nabla (u_h)_t)_K - \langle \hat{\mathbf{q}}_h \cdot \boldsymbol{\nu}, (u_h)_t \rangle_{\partial K} + \frac{1}{\varepsilon^2} (f(u_h), (u_h)_t)_K = 0, \quad (2.13)$$

$$((\mathbf{q}_h)_t, \mathbf{q}_h)_K + ((u_h)_t, \nabla \cdot \mathbf{q}_h)_K - \langle (\hat{u}_h)_t, \mathbf{q}_h \cdot \boldsymbol{\nu} \rangle_{\partial K} = 0. \quad (2.14)$$

Summing up Eqs. (2.13)-(2.14) and summing up over K , with the properties of the numerical flux (2.9), we can cancel the boundary terms and get

$$\frac{d}{dt} \left(\frac{1}{2} (\mathbf{q}_h, \mathbf{q}_h)_\Omega + \frac{1}{\varepsilon^2} (F(u_h), 1)_\Omega \right) + ((u_h)_t, (u_h)_t)_\Omega = 0, \quad (2.15)$$

which gives (2.11) obviously. Using Cauchy's inequality

$$\frac{d}{dt} (u_h, u_h)_\Omega = (u_h, 2(u_h)_t)_\Omega \leq \frac{1}{\epsilon} (u_h, u_h)_\Omega + \epsilon ((u_h)_t, (u_h)_t)_\Omega,$$

here ϵ is any positive constant. Take $\epsilon = 0.5$ and add the above two equations together to get

$$\frac{d}{dt} \left((u_h, u_h)_\Omega + \frac{1}{2}(\mathbf{q}_h, \mathbf{q}_h)_\Omega + \frac{1}{\epsilon^2}(F(u_h), 1)_\Omega \right) + \frac{1}{2}((u_h)_t, (u_h)_t)_\Omega \leq 2(u_h, u_h)_\Omega,$$

then

$$\frac{d}{dt} \left((u_h, u_h)_\Omega + \frac{1}{2}(\mathbf{q}_h, \mathbf{q}_h)_\Omega + \frac{1}{\epsilon^2}(F(u_h), 1)_\Omega \right) \leq 2(u_h, u_h)_\Omega.$$

The Gronwall's inequality is used to complete the proof

$$\begin{aligned} & \left((u_h, u_h)_\Omega + \frac{1}{2}(\mathbf{q}_h, \mathbf{q}_h)_\Omega + \frac{1}{\epsilon^2}(F(u_h), 1)_\Omega \right) (t) \\ & \leq e^{2t} \left((u_h, u_h)_\Omega + \frac{1}{2}(\mathbf{q}_h, \mathbf{q}_h)_\Omega + \frac{1}{\epsilon^2}(F(u_h), 1)_\Omega \right) (0). \end{aligned} \quad (2.16)$$

□

Remark 2.1. The proof of the energy stability is valid for the general form of $F(u) \geq 0$.

2.4. The semi-implicit time discretization method

Numerical simulations of the Allen-Cahn equation, using explicit methods, impose severe time step restrictions. It would therefore be desirable to develop implicit or semi-implicit time marching methods to alleviate the problem.

2.4.1. The nonlinearly stabilized convex splitting scheme

In this subsection, we will develop a convex splitting scheme for time discretization based on a convex splitting technique of the discrete Allen-Cahn energy for the typical form of $F(u)$ in (1.4). Coupled with the LDG spatial discretization, the fully-discrete LDG scheme is: Find $(u_h^{n+1}, \mathbf{q}_h^{n+1}) \in (V_h, \Sigma_h)$ such that, $\forall (\psi, \boldsymbol{\eta}) \in (V_h, \Sigma_h)$, we have

$$\left(\frac{u_h^{n+1} - u_h^n}{\Delta t}, \psi \right)_K + (\mathbf{q}_h^{n+1}, \nabla \psi)_K - \langle \hat{\mathbf{q}}_h^{n+1} \cdot \boldsymbol{\nu}, \psi \rangle_{\partial K} + \frac{1}{\epsilon^2}((u_h^{n+1})^3 - u_h^n, \psi)_K = 0, \quad (2.17a)$$

$$(\mathbf{q}_h^{n+1}, \boldsymbol{\eta})_K + (u_h^{n+1}, \nabla \cdot \boldsymbol{\eta})_K - \langle \hat{u}_h^{n+1}, \boldsymbol{\eta} \cdot \boldsymbol{\nu} \rangle_{\partial K} = 0. \quad (2.17b)$$

The numerical flux is defined as

$$\hat{\mathbf{q}}_h^{n+1}|_e = \mathbf{q}_{h,R}^{n+1}, \quad \hat{u}_h^{n+1}|_e = u_{h,L}^{n+1}. \quad (2.18)$$

Next, we will prove the unconditional energy stability for the fully-discrete LDG scheme (2.17) with the choice of the numerical fluxes (2.18). To simplify the notation, we use the following notations for discretization of time variable,

$$\delta_t u_h^{n+1} = \frac{u_h^{n+1} - u_h^n}{\Delta t},$$

$$\delta_t \mathbf{q}_h^{n+1} = \frac{\mathbf{q}_h^{n+1} - \mathbf{q}_h^n}{\Delta t}.$$

Proposition 2.2. *The solution to the fully-discrete LDG scheme (2.17) with the numerical fluxes (2.18) satisfies the discrete energy stability*

$$\frac{1}{2}(\mathbf{q}_h^{n+1}, \mathbf{q}_h^{n+1})_\Omega + \frac{1}{\varepsilon^2}(F(u_h^{n+1}), 1)_\Omega \leq \frac{1}{2}(\mathbf{q}_h^n, \mathbf{q}_h^n)_\Omega + \frac{1}{\varepsilon^2}(F(u_h^n), 1)_\Omega. \quad (2.19)$$

Proof. We choose the test functions $\psi = \delta_t u_h^{n+1}$ and $\boldsymbol{\eta} = \delta_t \mathbf{q}_h^{n+1}$ in Eqs. (2.17a) and (2.17b) of the scheme, and we get

$$\begin{aligned} & (\delta_t u_h^{n+1}, \delta_t u_h^{n+1})_K + (\mathbf{q}_h^{n+1}, \nabla \delta_t u_h^{n+1})_K - \langle \hat{\mathbf{q}}_h^{n+1} \cdot \boldsymbol{\nu}, \delta_t u_h^{n+1} \rangle_{\partial K} \\ & + \frac{1}{\varepsilon^2}((u_h^{n+1})^3 - u_h^n, \delta_t u_h^{n+1})_K = 0, \\ & (\mathbf{q}_h^{n+1}, \delta_t \mathbf{q}_h^{n+1})_K + (u_h^{n+1}, \nabla \cdot \delta_t \mathbf{q}_h^{n+1})_K - \langle \hat{u}_h^{n+1}, \delta_t \mathbf{q}_h^{n+1} \cdot \boldsymbol{\nu} \rangle_{\partial K} = 0. \end{aligned} \quad (2.20)$$

Summing up equations in (2.20), we obtain

$$\begin{aligned} & (\delta_t u_h^{n+1}, \delta_t u_h^{n+1})_K + (\mathbf{q}_h^{n+1}, \delta_t \mathbf{q}_h^{n+1})_K + \frac{1}{\varepsilon^2}((u_h^{n+1})^3 - u_h^n, \delta_t u_h^{n+1})_K \\ & = \frac{1}{\Delta t} (-(\mathbf{q}_h^{n+1}, \nabla u_h^{n+1})_K - (u_h^{n+1}, \nabla \cdot \mathbf{q}_h^{n+1})_K + \langle \hat{\mathbf{q}}_h^{n+1} \cdot \boldsymbol{\nu}, u_h^{n+1} \rangle_{\partial K} + \langle \hat{u}_h^{n+1}, \mathbf{q}_h^{n+1} \cdot \boldsymbol{\nu} \rangle_{\partial K}) \\ & + \frac{1}{\Delta t} ((\mathbf{q}_h^{n+1}, \nabla u_h^n)_K + (u_h^{n+1}, \nabla \cdot \mathbf{q}_h^n)_K - \langle \hat{\mathbf{q}}_h^{n+1} \cdot \boldsymbol{\nu}, u_h^n \rangle_{\partial K} - \langle \hat{u}_h^{n+1}, \mathbf{q}_h^n \cdot \boldsymbol{\nu} \rangle_{\partial K}). \end{aligned}$$

For Eq. (2.17b), we choose the test function as $\boldsymbol{\eta} = \mathbf{q}_h^n$, then we obtain

$$(\mathbf{q}_h^{n+1}, \mathbf{q}_h^n)_K + (u_h^{n+1}, \nabla \cdot \mathbf{q}_h^n)_K - \langle \hat{u}_h^{n+1}, \mathbf{q}_h^n \cdot \boldsymbol{\nu} \rangle_{\partial K} = 0. \quad (2.21)$$

From Eq. (2.17b), we have

$$(\mathbf{q}_h^n, \boldsymbol{\eta})_K + (u_h^n, \nabla \cdot \boldsymbol{\eta})_K - \langle \hat{u}_h^n, \boldsymbol{\eta} \cdot \boldsymbol{\nu} \rangle_{\partial K} = 0. \quad (2.22)$$

Choosing the test function $\boldsymbol{\eta} = \mathbf{q}_h^{n+1}$ in (2.22), we obtain

$$(\mathbf{q}_h^n, \mathbf{q}_h^{n+1})_K + (u_h^n, \nabla \cdot \mathbf{q}_h^{n+1})_K - \langle \hat{u}_h^n, \mathbf{q}_h^{n+1} \cdot \boldsymbol{\nu} \rangle_{\partial K} = 0. \quad (2.23)$$

Then we have

$$\begin{aligned} & (\mathbf{q}_h^{n+1}, \nabla u_h^n)_K + (u_h^{n+1}, \nabla \cdot \mathbf{q}_h^n)_K - \langle \hat{\mathbf{q}}_h^{n+1} \cdot \boldsymbol{\nu}, u_h^n \rangle_{\partial K} - \langle \hat{u}_h^{n+1}, \mathbf{q}_h^n \cdot \boldsymbol{\nu} \rangle_{\partial K} \\ & \stackrel{(2.21)}{=} -(\mathbf{q}_h^{n+1}, \mathbf{q}_h^n)_K + (\mathbf{q}_h^{n+1}, \nabla u_h^n)_K - \langle \hat{\mathbf{q}}_h^{n+1} \cdot \boldsymbol{\nu}, u_h^n \rangle_{\partial K} \\ & \stackrel{(2.23)}{=} (\mathbf{q}_h^{n+1}, \nabla u_h^n)_K - \langle \hat{\mathbf{q}}_h^{n+1} \cdot \boldsymbol{\nu}, u_h^n \rangle_{\partial K} + (u_h^n, \nabla \cdot \mathbf{q}_h^{n+1})_K - \langle \hat{u}_h^n, \mathbf{q}_h^{n+1} \cdot \boldsymbol{\nu} \rangle_{\partial K}. \end{aligned}$$

Summing up over K , with the properties of numerical flux (2.18), we can cancel the boundary terms and get

$$\begin{aligned} & (\delta_t u_h^{n+1}, \delta_t u_h^{n+1})_\Omega + (\mathbf{q}_h^{n+1}, \delta_t \mathbf{q}_h^{n+1})_\Omega + \frac{1}{\varepsilon^2}((u_h^{n+1})^3 - u_h^n, \delta_t u_h^{n+1})_\Omega \\ & = (\mathbf{q}_h^{n+1}, \delta_t \mathbf{q}_h^{n+1})_\Omega + \frac{1}{4\varepsilon^2 \Delta t}((1 - (u_h^{n+1})^2), 1)_\Omega - \frac{1}{4\varepsilon^2 \Delta t}((1 - (u_h^n)^2), 1)_\Omega \\ & + (\delta_t u_h^{n+1}, \delta_t u_h^{n+1})_\Omega + \frac{1}{4\varepsilon^2 \Delta t}((2 + 2(u_h^{n+1})^2 + (u_h^n + u_h^{n+1})^2)(u_h^n - u_h^{n+1})^2, 1)_\Omega \\ & = 0. \end{aligned}$$

Then we get

$$(\mathbf{q}_h^{n+1}, \delta_t \mathbf{q}_h^{n+1})_\Omega + \frac{1}{4\varepsilon^2 \Delta t} ((1 - (u_h^{n+1})^2)^2, 1)_\Omega - \frac{1}{4\varepsilon^2 \Delta t} ((1 - (u_h^n)^2)^2, 1)_\Omega \leq 0,$$

which implies the discrete energy stability result

$$\frac{1}{2}(\mathbf{q}_h^{n+1}, \mathbf{q}_h^{n+1})_\Omega + \frac{1}{\varepsilon^2}(F(u_h^{n+1}), 1)_\Omega \leq \frac{1}{2}(\mathbf{q}_h^n, \mathbf{q}_h^n)_\Omega + \frac{1}{\varepsilon^2}(F(u_h^n), 1)_\Omega.$$

2.4.2. The semi-implicit spectral deferred correction method □

The convex splitting scheme (2.17) is unconditionally energy stable, which means that it is stable regardless of time step size Δt . However, it is first order accurate in time. To improve the temporal accuracy, the spectral deferred correction (SDC) method will be employed. An advantage of this method is that it is a one step method and can be constructed easily and systematically for any order of accuracy.

Based on the convex splitting scheme (2.17), which can be rewritten as

$$u_h^{n+1} = u_h^n + \Delta t(F_N(u_h^n) + F_S(u_h^{n+1})) \quad (2.24)$$

for convenience, where $F_N(u_h)$ represents the explicit part and $F_S(u_h)$ represents the implicit part of the convex splitting scheme (2.17), *i.e.*

$$F_N(u_h) = \frac{1}{\varepsilon^2}u_h, \quad F_S(u_h) = \Delta u_h - \frac{1}{\varepsilon^2}u_h^3.$$

The SDC method is a one step, multi-stage method. Suppose now the time interval $[0, T]$ is divided into M intervals by the partition

$$0 = t_0 < t_1 < \dots < t_n < \dots < t_M = T.$$

Let $\Delta t_n = t_{n+1} - t_n$ and u_n denotes the numerical approximation of $u(t_n)$, with $u_0 = u(0)$. Then divide the time interval $[t_n, t_{n+1}]$ into P subintervals by choosing the points $t_{n,m}$ for $m = 0, 1, \dots, P$ such that

$$t_n = t_{n,0} < t_{n,1} < \dots < t_{n,m} < \dots < t_{n,P} = t_{n+1}.$$

Let $\Delta t_{n,m} = t_{n,m+1} - t_{n,m}$ and $u_{n,m}^k$ denotes the k^{th} order approximation to $u(t_{n,m})$. The points $\{t_{n,m}\}_{m=0}^P$ can be chosen to be the Chebyshev Gauss-Lobatto nodes on $[t_n, t_{n+1}]$ to avoid the instability of approximation at equispaced nodes for high order accuracy. We can also choose the Gauss nodes, or Legendre Gauss-Radau nodes or Legendre Gauss-Lobatto nodes. Starting from u_n , we give the algorithm to calculate u_{n+1} in the following.

Compute the initial approximation:

$$u_{n,0}^1 = u_n.$$

For our problem, use the convex splitting scheme (2.17) to compute a first order accurate approximate solution u^1 at the nodes $\{t_{n,m}\}_{m=1}^P$, *i.e.*

For $m = 0, \dots, P - 1$

$$u_{n,m+1}^1 = u_{n,m}^1 + \Delta t_{n,m}(F_N(t_{n,m}, u_{n,m}^1) + F_S(t_{n,m+1}, u_{n,m+1}^1)). \quad (2.25)$$

Compute successive corrections:For $k = 1, \dots, K$

$$u_{n,0}^{k+1} = u_n.$$

For $m = 0, \dots, P - 1$

$$u_{n,m+1}^{k+1} = u_{n,m}^{k+1} + \Delta t_{n,m} (F_N(t_{n,m}, u_{n,m}^{k+1}) - F_N(t_{n,m}, u_{n,m}^k) + F_S(t_{n,m+1}, u_{n,m+1}^{k+1}) - F_S(t_{n,m+1}, u_{n,m+1}^k)) + I_m^{m+1}(F_N(t, u^k) + F_S(t, u^k)), \quad (2.26)$$

where $I_m^{m+1}(F_N(t, u^k) + F_S(t, u^k))$ is the integral of the P -th degree interpolating polynomial on the $P + 1$ points

$$(t_{n,m}, F_N(t_{n,m}, u_{n,m}^k) + F_S(t_{n,m}, u_{n,m}^k))_{m=0}^P$$

over the subinterval $[t_{n,m}, t_{n,m+1}]$, which is the numerical quadrature approximation of

$$\int_{t_{n,m}}^{t_{n,m+1}} (F_N(\tau, u(\tau)) + F_S(\tau, u(\tau))) d\tau.$$

Finally we have $u_{n+1} = u_{n,P}^{K+1}$. For a detailed description of the method as well as their implementation and applications, we refer the readers to [12, 23, 28].

The use of the semi-implicit SDC method will typically result in nonlinear algebraic systems at each time step. We hope to provide an iterative solver that can efficiently solve the nonlinear systems. Traditional iterative methods such as nonlinear Gauss-Seidel method suffers from slow convergence rates, especially for large system. Following the work in [18], the FAS multigrid method [3] can be employed to solve the nonlinear systems. Numerical experiments in Section 4 will be given to show that the multigrid solver is efficient and the number of iterations is nearly independent of the problem size.

3. The Error Estimates of the LDG Method

In this section, we prove a priori error estimates in L^2 norm and the negative norm error estimates of the semi-discrete LDG scheme (2.8) for the Allen-Cahn equation with the typical form of $F(u)$ in (1.4). The proof is based on the rectangular meshes and we will first give some notations and projections on this special meshes.

3.1. Notations for different constants

To develop the necessary theory establishing for a priori error estimates, we outline the notations that will be used. We will adopt the following convention for different constants. These constants may have different values in each occurrence.

We will denote by C a positive constant independent of h , which may depends on the solution of the problem considered in this paper. For problems considered in this section, the exact solution is assumed to be smooth. Also, $0 \leq t \leq T$ for a fixed T . Therefore, the exact solution is always bounded.

3.2. Projections and interpolation properties

3.2.1. One-dimensional case

In what follows, we will consider the standard L^2 -projection of a function η with $k+1$ continuous derivatives into space V_h ,

$$P^\pm : H^1(\Omega) \longrightarrow V_h,$$

which are defined in the following form. Given a function $\eta \in H^1(\Omega)$ and an arbitrary subinterval $K_j = (x_{j-1}, x_j)$, the restriction of $P^\pm \eta$ to K_j are defined as the elements of $\mathcal{P}^k(K_j)$ that satisfy

$$\begin{aligned} \int_{K_j} (P^+ \eta - \eta) w dx &= 0, \quad \forall w \in \mathcal{P}^{k-1}(K_j), \quad \text{and} \quad P^+ \eta(x_{j-1}) = \eta(x_{j-1}), \\ \int_{K_j} (P^- \eta - \eta) w dx &= 0, \quad \forall w \in \mathcal{P}^{k-1}(K_j), \quad \text{and} \quad P^- \eta(x_j) = \eta(x_j). \end{aligned} \quad (3.1)$$

3.2.2. Two-dimensional case

To prove the error estimates for two-dimensional problems in Cartesian meshes, we need a suitable projection P^\pm similar to the one-dimensional case. The projections P^- for scalar functions are defined as

$$P^- = P_x^- \otimes P_y^-, \quad (3.2)$$

where the subscripts x and y indicate that the one-dimensional projections defined by (3.1) on a two-dimensional rectangle element

$$I \otimes J = [x_{j-1}, x_j] \times [y_{j-1}, y_j].$$

The projection Π^+ for vector-valued function $\boldsymbol{\rho} = (\rho_1(x, y), \rho_2(x, y))$ are defined as

$$\Pi^+ \boldsymbol{\rho} = (P_x^+ \otimes \pi_y \rho_1, \pi_x \otimes P_y^+ \rho_2), \quad (3.3)$$

where π_x and π_y are the standard L^2 projection in x and y direction, respectively. It is easy to see that, for any $\boldsymbol{\rho} \in [H^1(\Omega)]^2$, the restriction of $\Pi^+ \boldsymbol{\rho}$ to $I \otimes J$ are elements of $[\mathcal{Q}^k(I \otimes J)]^2$ that satisfy

$$\int_I \int_J (\Pi^+ \boldsymbol{\rho} - \boldsymbol{\rho}) \cdot \nabla w dy dx = 0, \quad (3.4)$$

for any $w \in \mathcal{Q}^k(I \otimes J)$, and

$$\int_J (\Pi^+ \boldsymbol{\rho}(x_{i-1}, y) - \boldsymbol{\rho}(x_{i-1}, y)) \cdot \boldsymbol{\nu} w(x_{i-1}^+, y) dy = 0 \quad \forall w \in \mathcal{Q}^k(I \otimes J), \quad (3.5)$$

$$\int_I (\Pi^+ \boldsymbol{\rho}(x, y_{j-1}) - \boldsymbol{\rho}(x, y_{j-1})) \cdot \boldsymbol{\nu} w(x, y_{j-1}^+) dy = 0 \quad \forall w \in \mathcal{Q}^k(I \otimes J), \quad (3.6)$$

where $\boldsymbol{\nu}$ is the normal vector of the domain integrated. For the definition of similar projection on three-dimensional case, we refer the readers to [10].

3.2.3. Interpolation properties

For the projections mentioned above, there are some approximation results for the projections (3.1), (3.2) and (3.3) in [8, 11]

$$\begin{aligned}\|\eta^e\|_\Omega + h^{\frac{1}{2}}\|\eta^e\|_\Gamma &\leq Ch^{k+1}\|\eta\|_{k+1,\Omega}, \quad \forall \eta \in H^{k+1}(\Omega), \\ \|\boldsymbol{\rho}^e\|_\Omega + h^{\frac{1}{2}}\|\boldsymbol{\rho}^e\|_\Gamma &\leq Ch^{k+1}\|\boldsymbol{\rho}\|_{k+1,\Omega}, \quad \forall \boldsymbol{\rho} \in [H^{k+1}(\Omega)]^d,\end{aligned}$$

where $\eta^e = \pi\eta - \eta$, $\boldsymbol{\rho}^e = \pi\boldsymbol{\rho} - \boldsymbol{\rho}$ or $\eta^e = P^\pm\eta - \eta$, $\boldsymbol{\rho}^e = \Pi^\pm\boldsymbol{\rho} - \boldsymbol{\rho}$ and C is independent of h .

The projection P^- on the Cartesian meshes has the following superconvergence property (see [10], Lemma 3.6).

Lemma 3.1. *Suppose $(\eta, \boldsymbol{\rho}) \in H^{k+2}(\Omega) \otimes \Sigma_h$ and the projection P^- is defined by (3.2), then we have*

$$|(\eta - P^-\eta, \nabla \cdot \boldsymbol{\rho})_\Omega - \langle \eta - \widehat{P^-\eta}, \boldsymbol{\rho} \cdot \boldsymbol{\nu} \rangle_\Gamma| \leq Ch^{k+1}\|\eta\|_{k+2,\Omega}\|\boldsymbol{\rho}\|_\Omega, \quad (3.7)$$

where “hat” term is numerical flux.

3.3. A priori error estimate in L^2 norm

In the previous section, the energy stability is presented. Now we concentrate on the derivation of an a priori error estimate in L^2 norm.

Theorem 3.2. (Error estimate in L^2 norm) *The solution u_h and \mathbf{q}_h of the semi-discrete LDG scheme (2.8) for the Eq. (1.1) with a smooth solution u and the initial condition $u_h(\mathbf{x}, 0) = P^-u(\mathbf{x}, 0)$ satisfy the error estimate*

$$\|u - u_h\|_\Omega^2 + \frac{1}{2}\varepsilon^2\|\mathbf{q} - \mathbf{q}_h\|_\Omega^2 + \frac{1}{4}\|(u - u_h)^2\|_\Omega^2 \leq Ch^{2k+2}, \quad (3.8)$$

where C depends on $\|f'\|_{L^\infty(\Omega)}$, ε , T , $\|u\|_{L^\infty([0,T];H^{k+2}(\Omega))}$ but is independent of h .

Proof. First, it is obvious that the exact solution of (1.1) also satisfies the LDG scheme (2.8), which gives the following error equations

$$(u_t - (u_h)_t, \psi)_K + (\mathbf{q} - \mathbf{q}_h, \nabla \psi)_K - \langle (\mathbf{q} - \hat{\mathbf{q}}_h) \cdot \boldsymbol{\nu}, \psi \rangle_{\partial K} + \frac{1}{\varepsilon^2}(f(u) - f(u_h), \psi)_K = 0, \quad (3.9a)$$

$$(\mathbf{q} - \mathbf{q}_h, \boldsymbol{\eta})_K + (u - u_h, \nabla \cdot \boldsymbol{\eta})_K - \langle u - \hat{u}_h, \boldsymbol{\eta} \cdot \boldsymbol{\nu} \rangle_{\partial K} = 0. \quad (3.9b)$$

Denote

$$e_u = u - u_h, \quad e_q = \mathbf{q} - \mathbf{q}_h.$$

Add and subtract projections Pu and $\Pi\mathbf{q}$, now the error can be divided into

$$e_u = u - u_h = u - Pu + Pu - u_h = u - Pu + Pe_u, \quad (3.10)$$

$$e_q = \mathbf{q} - \mathbf{q}_h = \mathbf{q} - \Pi\mathbf{q} + \Pi\mathbf{q} - \mathbf{q}_h = \mathbf{q} - \Pi\mathbf{q} + \Pi e_q. \quad (3.11)$$

Let P and Π be the projections onto the finite element spaces V_h and Σ_h , respectively, which have been defined in Section 2.1. We choose the projection as follows

$$(P, \Pi) = (P^-, P^+), \quad \text{in one-dimension,} \quad (3.12)$$

$$(P, \Pi) = (P^-, \Pi^+), \quad \text{in multi-dimension.} \quad (3.13)$$

We choose the initial condition $u_h(\mathbf{x}, 0) = P^-u(\mathbf{x}, 0)$. By Eq. (3.9b) and Lemma 3.1, we obtain the initial error estimates

$$\begin{aligned} \|u(\mathbf{x}, 0) - u_h(\mathbf{x}, 0)\|_{\Omega} &\leq Ch^{k+1}, \\ \|\mathbf{q}(\mathbf{x}, 0) - \mathbf{q}_h(\mathbf{x}, 0)\|_{\Omega} &\leq Ch^{k+1}. \end{aligned} \quad (3.14)$$

We will mimic the idea of the choice of the test functions in the proof of energy stability. Taking $\psi = Pe_{u_t}$ and $\boldsymbol{\eta} = \Pi e_{\mathbf{q}}$ in Eqs. (3.9a) and (3.9b), respectively, we have

$$(Pe_{u_t}, Pe_{u_t})_K + (\Pi e_{\mathbf{q}_t}, \Pi e_{\mathbf{q}})_K + \frac{1}{\varepsilon^2}(f(u) - f(u_h), Pe_{u_t})_K = RHS,$$

where

$$\begin{aligned} RHS &= -(u_t - Pu_t, Pe_{u_t})_K - (\mathbf{q} - \Pi \mathbf{q}, \nabla Pe_{u_t})_K + \langle (\mathbf{q} - \widehat{\Pi \mathbf{q}}) \cdot \boldsymbol{\nu}, Pe_{u_t} \rangle_{\partial K} \\ &\quad - (\mathbf{q}_t - \Pi \mathbf{q}_t, \Pi e_{\mathbf{q}})_K - (u_t - Pu_t, \nabla \cdot \Pi e_{\mathbf{q}})_K + \langle u_t - \widehat{Pu_t}, \Pi e_{\mathbf{q}} \cdot \boldsymbol{\nu} \rangle_{\partial K} \\ &\quad - (\Pi e_{\mathbf{q}}, \nabla Pe_{u_t})_K + \langle \widehat{\Pi e_{\mathbf{q}}} \cdot \boldsymbol{\nu}, Pe_{u_t} \rangle_{\partial K} - (Pe_{u_t}, \nabla \cdot \Pi e_{\mathbf{q}})_K + \langle \widehat{Pe_{u_t}}, \Pi e_{\mathbf{q}} \cdot \boldsymbol{\nu} \rangle_{\partial K}. \end{aligned}$$

Summing up over K , using the flux (2.9) and the property of projections, it is possible to show that

$$(Pe_{u_t}, Pe_{u_t})_{\Omega} + (\Pi e_{\mathbf{q}_t}, \Pi e_{\mathbf{q}})_{\Omega} + \frac{1}{\varepsilon^2}(f(u) - f(u_h), Pe_{u_t})_{\Omega} = RHS, \quad (3.15)$$

where

$$\begin{aligned} RHS &= - \sum_K (u_t - Pu_t, Pe_{u_t})_K - \sum_K (\mathbf{q}_t - \Pi \mathbf{q}_t, \Pi e_{\mathbf{q}})_K \\ &\quad + \sum_K (-(u_t - Pu_t, \nabla \cdot \Pi e_{\mathbf{q}})_K + \langle u_t - \widehat{Pu_t}, \Pi e_{\mathbf{q}} \cdot \boldsymbol{\nu} \rangle_{\partial K}). \end{aligned}$$

By Cauchy-Schwarz inequality and Lemma 3.1, the RHS is bounded by the following inequality

$$\begin{aligned} |RHS| &\leq \|u_t - Pu_t\|_{\Omega} \|Pe_{u_t}\|_{\Omega} + \|\mathbf{q}_t - \Pi \mathbf{q}_t\|_{\Omega} \|\Pi e_{\mathbf{q}}\|_{\Omega} + Ch^{k+1} \|\Pi e_{\mathbf{q}}\|_{\Omega} \\ &\leq Ch^{k+1} (\|Pe_{u_t}\|_{\Omega} + \|\Pi e_{\mathbf{q}}\|_{\Omega}) \\ &\leq Ch^{2k+2} + \frac{1}{8} \|Pe_{u_t}\|_{\Omega}^2 + \frac{1}{2} \|\Pi e_{\mathbf{q}}\|_{\Omega}^2, \end{aligned} \quad (3.16)$$

where C is a positive constant dependent on $\|u\|_{L^{\infty}([0, T]; H^{k+2}(\Omega))}$, but independent of h .

For now we assume $f(u) = u^3 - u$, a direct calculation gives

$$f(u) - f(u_h) = f'(u)(u - u_h) + (u - u_h)^3 + 3u(u - u_h)^2, \quad (3.17)$$

where $f'(u) = 3u^2 - 1$ is the derivative of $f(u)$. Consider the nonlinear term

$$\begin{aligned} &\frac{1}{\varepsilon^2}(f(u) - f(u_h), Pe_{u_t})_{\Omega} \\ &= \frac{1}{\varepsilon^2}(f(u) - f(Pu), Pe_{u_t})_{\Omega} + \frac{1}{\varepsilon^2}(f(Pu) - f(u_h), Pe_{u_t})_{\Omega} \\ &= \frac{1}{\varepsilon^2}(f'(\xi)(u - Pu), Pe_{u_t})_{\Omega} + \frac{1}{\varepsilon^2}(f(Pu) - f(u_h), Pe_{u_t})_{\Omega} \end{aligned}$$

$$=(I) + (II),$$

where ξ is between u and Pu . For any positive constant $\epsilon > 0$, using Cauchy's inequality, (I) is bounded by

$$\begin{aligned} |(I)| &\leq \frac{1}{\epsilon^2} \|f'\|_{L^\infty(\Omega)} |(u - Pu, Pe_{u_t})_\Omega| \\ &\leq \frac{1}{\epsilon^2} \left(\epsilon \|Pe_{u_t}\|_\Omega^2 + \frac{\|f'\|_{L^\infty(\Omega)}^2}{4\epsilon} \|u - Pu\|_\Omega^2 \right). \end{aligned}$$

Taking $\epsilon = \frac{1}{4}\epsilon^2$

$$|(I)| \leq \frac{1}{4} \|Pe_{u_t}\|_\Omega^2 + \frac{C}{\epsilon^4} h^{2k+2}, \quad (3.18)$$

where C is a positive constant dependent on $\|f'\|_{L^\infty(\Omega)}$ and $\|u\|_{k+1,\Omega}$, but independent of h . Using (3.17), (II) can be rewritten as

$$\begin{aligned} (II) &= \frac{1}{\epsilon^2} (f'(Pu)(Pu - u_h) + (Pu - u_h)^3 + 3Pu(Pu - u_h)^2, Pe_{u_t})_\Omega \\ &= \frac{1}{\epsilon^2} (f'(Pu)Pe_u + (Pe_u)^3 + 3Pu(Pe_u)^2, Pe_{u_t})_\Omega \\ &= \frac{1}{4\epsilon^2} \frac{d}{dt} ((Pe_u)^2, (Pe_u)^2)_\Omega + \frac{1}{\epsilon^2} (f'(Pu)Pe_u + 3Pu(Pe_u)^2, Pe_{u_t})_\Omega \\ &= \frac{1}{4\epsilon^2} \frac{d}{dt} ((Pe_u)^2, (Pe_u)^2)_\Omega + (III). \end{aligned} \quad (3.19)$$

For (III), it is obvious that

$$|(III)| \leq \frac{1}{4} \|Pe_{u_t}\|_\Omega^2 + \frac{C}{\epsilon^4} (\|Pe_u\|_\Omega^2 + ((Pe_u)^2, (Pe_u)^2)_\Omega). \quad (3.20)$$

Combining Eqs. (3.15), (3.16), (3.18), (3.19) and (3.20), we have

$$\begin{aligned} \|Pe_{u_t}\|_\Omega^2 + \frac{1}{2} \frac{d}{dt} \|\Pi e_{\mathbf{q}}\|_\Omega^2 &\leq -\frac{1}{4\epsilon^2} \frac{d}{dt} \|(Pe_u)^2\|_\Omega^2 + \frac{5}{8} \|Pe_{u_t}\|_\Omega^2 + \frac{1}{2} \|\Pi e_{\mathbf{q}}\|_\Omega^2 \\ &\quad + \frac{C}{\epsilon^4} (\|(Pe_u)^2\|_\Omega^2 + \|Pe_u\|_\Omega^2) + Ch^{2k+2} + \frac{C}{\epsilon^4} h^{2k+2}. \end{aligned}$$

Using Cauchy's inequality

$$\frac{d}{dt} \left(\frac{1}{\epsilon^2} \|Pe_u\|_\Omega^2 \right) \leq \frac{1}{\epsilon^2} \left(\frac{1}{\eta} \|Pe_u\|_\Omega^2 + \eta \|Pe_{u_t}\|_\Omega^2 \right).$$

Take $\eta = \frac{1}{8}\epsilon^2$ and add the above two equations together to get

$$\begin{aligned} &\frac{d}{dt} \left(\frac{1}{\epsilon^2} \|Pe_u\|_\Omega^2 + \frac{1}{2} \|\Pi e_{\mathbf{q}}\|_\Omega^2 + \frac{1}{4\epsilon^2} \|(Pe_u)^2\|_\Omega^2 \right) \\ &\leq \frac{1}{2} \|\Pi e_{\mathbf{q}}\|_\Omega^2 + \frac{C}{\epsilon^4} (\|Pe_u\|_\Omega^2 + \|(Pe_u)^2\|_\Omega^2) + Ch^{2k+2} + \frac{C}{\epsilon^4} h^{2k+2}. \end{aligned}$$

Multiply ϵ^2 by both sides of the inequality and use the Gronwall's inequality and the initial error estimates (3.14) finally give us the error estimate

$$\|u - u_h\|_\Omega^2 + \frac{1}{2} \epsilon^2 \|\mathbf{q} - \mathbf{q}_h\|_\Omega^2 + \frac{1}{4} \|(u - u_h)^2\|_\Omega^2 \leq Ch^{2k+2},$$

where C depends on e^{T/ϵ^2} . □

3.4. Negative order norm estimate

In this section, we will show the approximate solution, $u_h(T)$, converges with higher order in the negative order norm.

Theorem 3.3. (Error estimate in the negative-order norm) *Let u_h be the approximate solution of the Allen-Cahn equation (1.1) given by the LDG scheme (2.8). Assuming that the initial data u_0 is smooth enough, if the finite element space is the piecewise polynomials of degree $k \geq 1$, we then have the following error estimate in negative-order norm*

$$\|u - u_h\|_{-(k+1),\Omega} \leq Ch^{2k+1}, \quad (3.21)$$

where C depends on $\|u_0\|_{k+1,\Omega}$, $\|u\|_{L^\infty([0,T];H^{k+2}(\Omega))}$, $\|f''\|_{L^\infty(\Omega)}$, ε and T , but independent of h .

Proof. We now show, for a given time T , our LDG approximate solution, u_h , converges with higher order in the negative-order norm by employing a dual argument, which is commonly used to obtain low-order norm in the finite element methods. Given that $\ell > 0$, we wish to estimate error

$$\|u(T) - u_h(T)\|_{-\ell,\Omega} = \sup_{\Phi \in C_0^\infty(\Omega)} \frac{(u(T) - u_h(T), \Phi)_\Omega}{\|\Phi\|_{\ell,\Omega}}. \quad (3.22)$$

And our dual equation is defined as: Find a function φ such that $\varphi(\cdot, t)$ is 1-periodic for all $t \in [0, T)$ and

$$\varphi_t + \Delta\varphi - \frac{1}{\varepsilon^2}f'(u)\varphi = 0, \quad \Omega \times (0, T), \quad (3.23a)$$

$$\varphi(\mathbf{x}, T) = \Phi. \quad (3.23b)$$

Multiply (1.1) by φ and (3.23a) by u to get

$$\frac{d}{dt}(u, \varphi)_\Omega = -\frac{1}{\varepsilon^2}(f(u), \varphi)_\Omega + \frac{1}{\varepsilon^2}(f'(u)u, \varphi)_\Omega. \quad (3.24)$$

This relation allows us to estimate the term $(u(T) - u_h(T), \Phi)_\Omega$ appearing in the definition of the negative order norm (3.22). That is

$$\begin{aligned} (u - u_h, \Phi)_\Omega(T) &= (u, \varphi)_\Omega(T) - (u_h, \varphi)_\Omega(T) \\ &= (u - u_h, \varphi)_\Omega(0) + \frac{1}{\varepsilon^2} \int_0^T (-(f(u), \varphi)_\Omega + (f'(u)u, \varphi)_\Omega) dt \\ &\quad - \int_0^T ((u_h)_t, \varphi)_\Omega + (u_h, \varphi_t)_\Omega dt. \end{aligned}$$

For Eq. (2.8), summing up over K , we get

$$((u_h)_t, \psi)_\Omega + B_1(\mathbf{q}_h, u_h; \psi) = 0, \quad (3.25a)$$

$$(\mathbf{q}_h, \boldsymbol{\eta})_\Omega + B_2(u_h; \boldsymbol{\eta}) = 0, \quad (3.25b)$$

where the bilinear forms B_1, B_2 are defined as

$$B_1(\mathbf{q}_h, u_h; \psi) = \sum_K (\mathbf{q}_h, \nabla\psi)_K - \sum_K \langle \hat{\mathbf{q}}_h \cdot \boldsymbol{\nu}, \psi \rangle_{\partial K} + \frac{1}{\varepsilon^2}(f(u_h), \psi)_\Omega, \quad (3.26)$$

$$B_2(u_h; \boldsymbol{\eta}) = \sum_K (u_h, \nabla \cdot \boldsymbol{\eta})_K - \sum_K \langle \hat{u}_h, \boldsymbol{\eta} \cdot \boldsymbol{\nu} \rangle_{\partial K}. \quad (3.27)$$

Consider the term $((u_h)_t, \varphi)_\Omega$,

$$\begin{aligned} ((u_h)_t, \varphi)_\Omega &= ((u_h)_t, \varphi - P\varphi)_\Omega + B_1(\mathbf{q}_h, u_h; \varphi - P\varphi) - B_1(\mathbf{q}_h, u_h; \varphi) \\ &= ((u_h)_t, \varphi - P\varphi)_\Omega + B_1(\mathbf{q}_h, u_h; \varphi - P\varphi) - (\mathbf{q}_h, \nabla \varphi)_\Omega - \frac{1}{\varepsilon^2} (f(u_h), \varphi)_\Omega \\ &= ((u_h)_t, \varphi - P\varphi)_\Omega + B_1(\mathbf{q}_h, u_h; \varphi - P\varphi) - (\mathbf{q}_h, \nabla \varphi - \Pi(\nabla \varphi))_\Omega \\ &\quad - B_2(u_h; \nabla \varphi - \Pi(\nabla \varphi)) + (u_h, \Delta \varphi)_\Omega - \frac{1}{\varepsilon^2} (f(u_h), \varphi)_\Omega, \end{aligned}$$

where P and Π are standard L^2 projections. Now it is possible to rewrite

$$\begin{aligned} &((u_h)_t, \varphi)_\Omega + (u_h, \varphi_t)_\Omega + \frac{1}{\varepsilon^2} (f(u), \varphi)_\Omega - \frac{1}{\varepsilon^2} (f'(u)u, \varphi)_\Omega \\ &= ((u_h)_t, \varphi - P\varphi)_\Omega + B_1(\mathbf{q}_h, u_h; \varphi - P\varphi) \\ &\quad - (\mathbf{q}_h, \nabla \varphi - \Pi(\nabla \varphi))_\Omega - B_2(u_h; \nabla \varphi - \Pi(\nabla \varphi)) \\ &\quad + (u_h, \Delta \varphi)_\Omega - \frac{1}{\varepsilon^2} (f(u_h), \varphi)_\Omega + (u_h, \varphi_t)_\Omega + \frac{1}{\varepsilon^2} (f(u), \varphi)_\Omega - \frac{1}{\varepsilon^2} (f'(u)u, \varphi)_\Omega. \end{aligned}$$

Denote

$$\Theta_1 = (u - u_h, \varphi)_\Omega(0),$$

$$\Theta_2 = - \int_0^T (((u_h)_t, \varphi - P\varphi)_\Omega + B_1(\mathbf{q}_h, u_h; \varphi - P\varphi)) dt,$$

$$\Theta_3 = \int_0^T ((\mathbf{q}_h, \nabla \varphi - \Pi(\nabla \varphi))_\Omega + B_2(u_h; \nabla \varphi - \Pi(\nabla \varphi))) dt,$$

$$\Theta_4 = - \int_0^T \left((u_h, \Delta \varphi)_\Omega - \frac{1}{\varepsilon^2} (f(u_h), \varphi)_\Omega + (u_h, \varphi_t)_\Omega + \frac{1}{\varepsilon^2} (f(u), \varphi)_\Omega - \frac{1}{\varepsilon^2} (f'(u)u, \varphi)_\Omega \right) dt.$$

Thus, now we have

$$(u - u_h, \Phi)_\Omega(T) = \Theta_1 + \Theta_2 + \Theta_3 + \Theta_4.$$

By the results in the convection diffusion equations [19], we have

$$|\Theta_1| \leq C_1 h^{2k+2} \|u_0\|_{k+1, \Omega} \|\varphi(0)\|_{k+1, \Omega}, \quad (3.28)$$

$$|\Theta_2| \leq C_2 h^{2k+1} \left(\int_0^T \|\varphi\|_{k+1, \Omega} dt \right)^{1/2}, \quad (3.29)$$

$$|\Theta_3| \leq C_3 h^{2k+1} \left(\int_0^T \|\varphi\|_{k+2, \Omega} dt \right)^{1/2}. \quad (3.30)$$

Now the only left thing is to estimate Θ_4 . With the help of dual equation,

$$\begin{aligned} \Theta_4 &= - \int_0^T \left((u_h, \Delta \varphi + \varphi_t)_\Omega - \frac{1}{\varepsilon^2} (f(u_h), \varphi)_\Omega + \frac{1}{\varepsilon^2} (f(u), \varphi)_\Omega - \frac{1}{\varepsilon^2} (f'(u)u, \varphi)_\Omega \right) dt \\ &= - \frac{1}{\varepsilon^2} \int_0^T \left((u_h, f'(u)\varphi)_\Omega - (f(u_h), \varphi)_\Omega + (f(u), \varphi)_\Omega - (f'(u)u, \varphi)_\Omega \right) dt \end{aligned}$$

$$\begin{aligned}
&= -\frac{1}{\varepsilon^2} \int_0^T (-f(u_h) + f(u) + f'(u)(u_h - u), \varphi)_\Omega dt \\
&= -\frac{1}{\varepsilon^2} \int_0^T \left(\frac{1}{2} (-f''(\eta)(u_h - u)^2, \varphi)_\Omega \right) dt,
\end{aligned}$$

where η is between u and u_h . From the results of error estimates for u_h and the inverse inequality [8], we know that $\|u_h\|_\infty$ is bounded when $k \geq 1$. Thus, we have

$$\begin{aligned}
|\Theta_4| &\leq \frac{1}{2\varepsilon^2} \|f''\|_{L^\infty(\Omega)} \|\varphi\|_{L^\infty(\Omega)} \|u - u_h\|_\Omega^2 \\
&\leq Ch^{2k+2} \|\varphi\|_{L^\infty(\Omega)} \stackrel{k \geq 1}{\leq} Ch^{2k+2} \|\varphi\|_{k+1, \Omega}.
\end{aligned} \tag{3.31}$$

For the last inequality, we use Sobolev inequality [4] which requires $k \geq 1$. Combining Eqs. (3.28)-(3.31), we get the negative order norm estimate

$$\|u - u_h\|_{-(k+1), \Omega} \leq Ch^{2k+1}. \tag{3.32}$$

Remark 3.1. This negative norm error estimate is very essential in the accuracy enhancement post-processing technique [19, 20]. We will also show the numerical results in Section 4 of the post-processing. \square

4. Numerical Tests

In this section, we present numerical results to confirm that we can indeed get the optimal convergence rate of $\mathcal{O}(h^{k+1})$ in L^2 norm and also improve the LDG solution from $\mathcal{O}(h^{k+1})$ to $\mathcal{O}(h^{2k+1})$ with the accuracy enhancement post-processing technique. All the examples are calculated by the LDG spatial discretization and the semi-implicit SDC time marching method except for Example 4.2 (convex splitting scheme). With this semi-implicit time discretization method, the time step can be chosen as $\Delta t = O(\Delta x)$, which is more larger than explicit methods. The resulting nonlinear systems are solved by the multigrid solver and we show numerically that the method has nearly mesh-independent convergence rates. All the computations are performed in double precision and uniform meshes. The L^2 error is computed using a six-point Gauss quadrature rule and the L^∞ error is calculated using the same six Gauss points in each element for all elements.

Example 4.1. We begin by considering the Allen-Cahn equation

$$u_t - \Delta u + \frac{1}{\varepsilon^2} f(u) = g(x, y, t) \tag{4.1}$$

with periodic boundary conditions and $\varepsilon = 0.3$ on the domain $\Omega = [0, 2\pi] \times [0, 2\pi]$. The forcing function $g(x, y, t)$ is taken to make the exact solution $u(x, y, t) = e^{-2t} \sin(x + y)$. The errors are presented in Table 4.1 and are computed at time $T = 0.5$. We clearly see that we can improve the order of the error from $\mathcal{O}(h^{k+1})$ to at least $\mathcal{O}(h^{2k+1})$ in both the L^2 - and L^∞ - norms after post-processing.

To illustrate the superiority of the multigrid solver, we present the convergence rates of the method for a single time step by using \mathcal{P}^1 and \mathcal{P}^2 approximation. From Fig. 4.1, we can see that each iteration of the multigrid solver is an $O(N)$ operation. We also clearly see that the convergence behavior of the multigrid method with Gauss-Seidel smoother is much better than with Jacobi smoother, thus we further restrict our study to the former.

Table 4.1: L^2 - and L^∞ -errors for Example 4.1 before and after post-processing at time $T = 0.5$ using the LDG method.

Mesh	Before post-processing				After post-processing			
	L^2 error	order	L^∞ error	order	L^2 error	order	L^∞ error	order
\mathcal{P}^1								
16	3.26E-002	–	2.58E-002	–	1.24E-002	–	2.99E-003	–
32	7.57E-003	2.11	6.73E-003	1.94	5.01E-004	4.63	1.19E-004	4.65
64	1.88E-003	2.00	1.69E-003	1.99	1.81E-005	4.79	4.03E-006	4.89
\mathcal{P}^2								
16	2.19E-003	–	2.55E-003	–	2.71E-004	–	6.88E-005	–
32	2.69E-004	3.02	3.08E-004	3.05	2.66E-006	6.67	6.93E-007	6.63
64	3.36E-005	3.00	3.83E-005	3.00	3.04E-008	6.45	7.74E-009	6.48
\mathcal{P}^3								
16	1.09E-004	–	1.41E-004	–	2.29E-006	–	5.02E-007	–
32	6.82E-006	4.00	8.82E-006	4.00	9.47E-009	7.92	2.43E-009	7.69
64	4.26E-007	4.00	5.51E-007	4.00	5.73E-011	7.37	1.40E-011	7.44

Table 4.2: L^2 - and L^∞ -errors for Example 4.2 at time $T = 0.5$ with different time steps.

N	$\Delta t = 0.1\Delta x$				$\Delta t = 0.5\Delta x$			
	L^2 error	order	L^∞ error	order	L^2 error	order	L^∞ error	order
16	1.15E-00	–	3.03E-01	–	1.85E-00	–	4.28E-01	–
32	7.37E-01	0.65	1.77E-01	0.77	1.45E-00	0.35	3.14E-01	0.45
64	4.41E-01	0.74	1.01E-01	0.80	1.09E-00	0.40	2.29E-01	0.46
128	2.46E-01	0.84	5.56E-02	0.87	7.74E-01	0.50	1.59E-01	0.53
$\Delta t = 2.5\Delta x$								
N	L^2 error	order	L^∞ error	order	L^2 error	order	L^∞ error	order
16	2.48E-00	–	5.84E-01	–	2.48E-00	–	5.84E-01	–
32	2.40E-00	0.05	5.46E-01	0.09	2.46E-00	–	5.73E-01	–
64	1.93E-00	0.31	4.14E-01	0.40	2.39E-00	0.04	5.41E-01	0.08
128	1.54E-00	0.33	3.16E-01	0.39	1.93E-00	0.31	4.11E-01	0.40

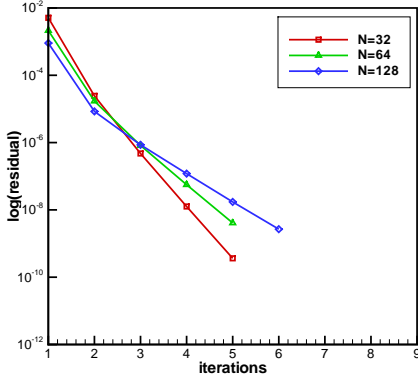
Example 4.2. We consider the Allen-Cahn equation (4.1) with the convex splitting scheme (2.17) in $\Omega = [0, 2\pi] \times [0, 2\pi]$ with $\varepsilon = 0.3$ and periodic boundary conditions.

The convex splitting scheme (2.17) is first order accurate in time, so we just consider \mathcal{P}^0 approximation. The L^2 and L^∞ errors, and the numerical order of accuracy at time $T = 0.5$ with different time steps are presented in Table 4.2. The numerical experiments go well with the theoretical result of the unconditional energy stability for the scheme. That is, as time step increases, the scheme is stable, but the error and accurate will be destroyed.

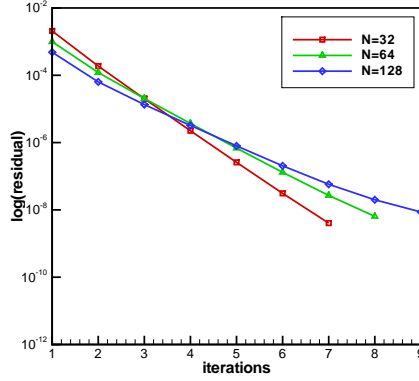
Example 4.3. We consider

$$u_t - \varepsilon^2 \Delta u + f(u) = g(x, y, t) \quad (4.2)$$

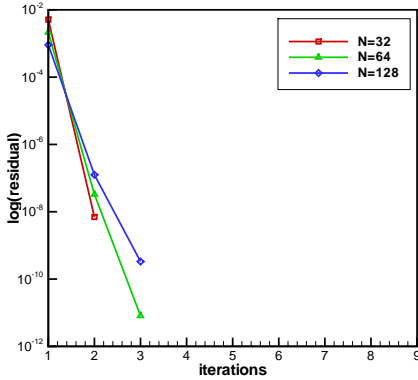
with $\varepsilon = 0.1$ in $\Omega = [0, 2\pi] \times [0, 2\pi]$ and periodic boundary conditions. We take the exact solution of $u(x, y, t) = e^{-2\varepsilon^2 t} \sin(x) \sin(y)$ with the source term $g(x, y, t)$, where $g(x, y, t)$ is a given function so that make the exact solution. The L^2 and L^∞ errors and the numerical orders



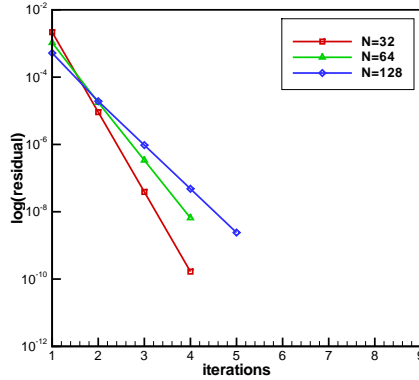
(a) \mathcal{P}^1 approximation with Jacobi smoother



(b) \mathcal{P}^2 approximation with Jacobi smoother



(c) \mathcal{P}^1 approximation with Gauss-Seidel smoother



(d) \mathcal{P}^2 approximation with Gauss-Seidel smoother

Fig. 4.1. Convergence rates of multigrid solver for \mathcal{P}^1 and \mathcal{P}^2 approximation for Example 4.1.

of accuracy before and after post-processing at time $T = 0.5$ are contained in Table 4.3. It is clear that we can improve on the LDG scheme from $\mathcal{O}(h^{k+1})$ to at least $\mathcal{O}(h^{2k+1})$.

Example 4.4. We seek traveling wave solutions for equation

$$u_t - \varepsilon^2 u_{xx} + f(u) = 0 \tag{4.3}$$

as

$$u(x, t) = \frac{1}{2} \left(1 - \tanh\left(\frac{x - st}{2\sqrt{2}\varepsilon}\right) \right), \tag{4.4}$$

where s is the speed of the traveling wave and $s = 3\varepsilon/\sqrt{2}$, $\varepsilon = 0.05$. We apply the LDG method to Eq. (4.3) in domain $\Omega = [-0.5, 1.5]$ with Neumann boundary conditions. The final time is $T = 1/s$ and the numerical traveling wave solutions with an initial profile, $u(x, 0) = \frac{1}{2}(1 - \tanh(\frac{x}{2\sqrt{2}\varepsilon}))$ and exact solution (4.4) are shown in Fig. 4.2.

Example 4.5. We consider the equation

$$u_t - \Delta u + \frac{1}{\varepsilon^2} f(u) = 0 \tag{4.5}$$

Table 4.3: L^2 - and L^∞ -errors for Example 4.3 before and after post-processing at time $T = 0.5$ using the LDG method.

Mesh	Before post-processing				After post-processing			
	L^2 error	order	L^∞ error	order	L^2 error	order	L^∞ error	order
\mathcal{P}^1								
16	5.11E-002	–	3.26E-002	–	2.43E-003	–	9.74E-004	–
32	1.40E-002	1.86	9.43E-003	1.79	1.69E-004	3.84	7.55E-005	3.69
64	3.57E-003	1.98	2.52E-003	1.90	1.10E-005	3.94	5.25E-006	3.85
\mathcal{P}^2								
16	3.57E-003	–	3.23E-003	–	7.89E-005	–	2.73E-005	–
32	4.59E-004	2.96	4.24E-004	2.93	1.37E-006	5.84	4.72E-007	5.86
64	5.71E-005	3.01	5.21E-005	3.02	3.04E-008	5.50	9.04E-09	5.71
\mathcal{P}^3								
16	1.73E-004	–	1.88E-004	–	3.56E-006	–	1.15E-006	–
32	1.13E-005	3.93	1.39E-005	3.75	1.44E-008	7.94	4.69E-09	7.94
64	7.15E-007	3.99	9.17E-007	3.93	5.84E-011	7.95	1.88E-011	7.96

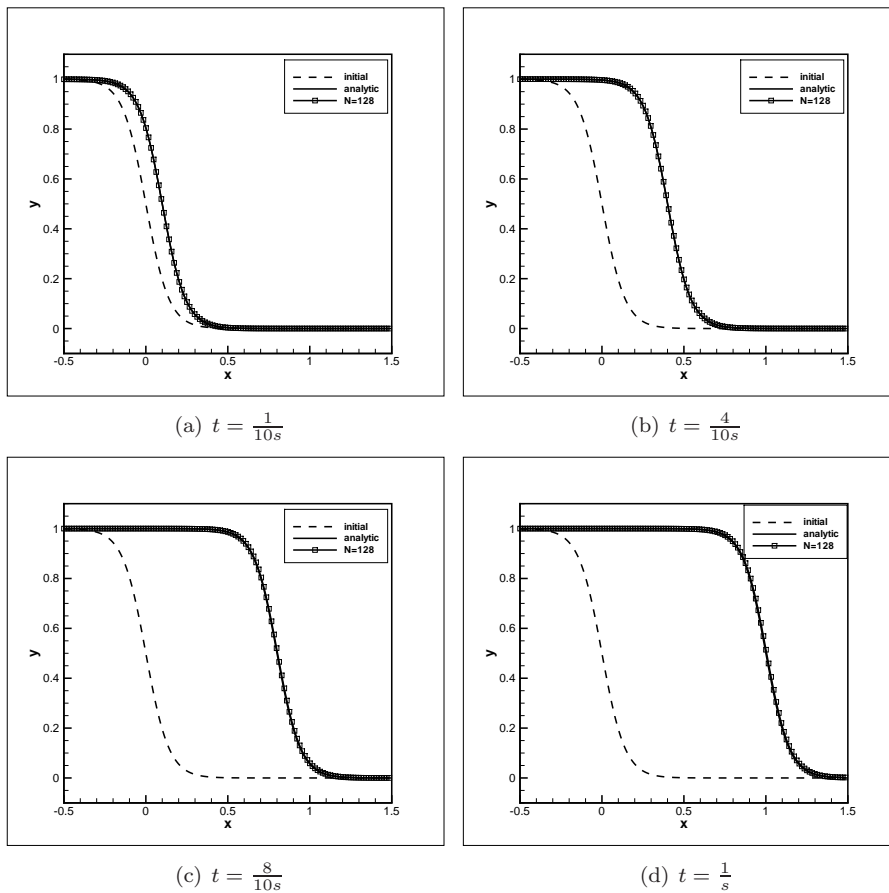


Fig. 4.2. Numerical traveling wave solutions at different times with an initial profile, $u(x, 0) = \frac{1}{2}(1 - \tanh(\frac{x}{2\sqrt{2}\epsilon}))$. The final time is $1/s$.

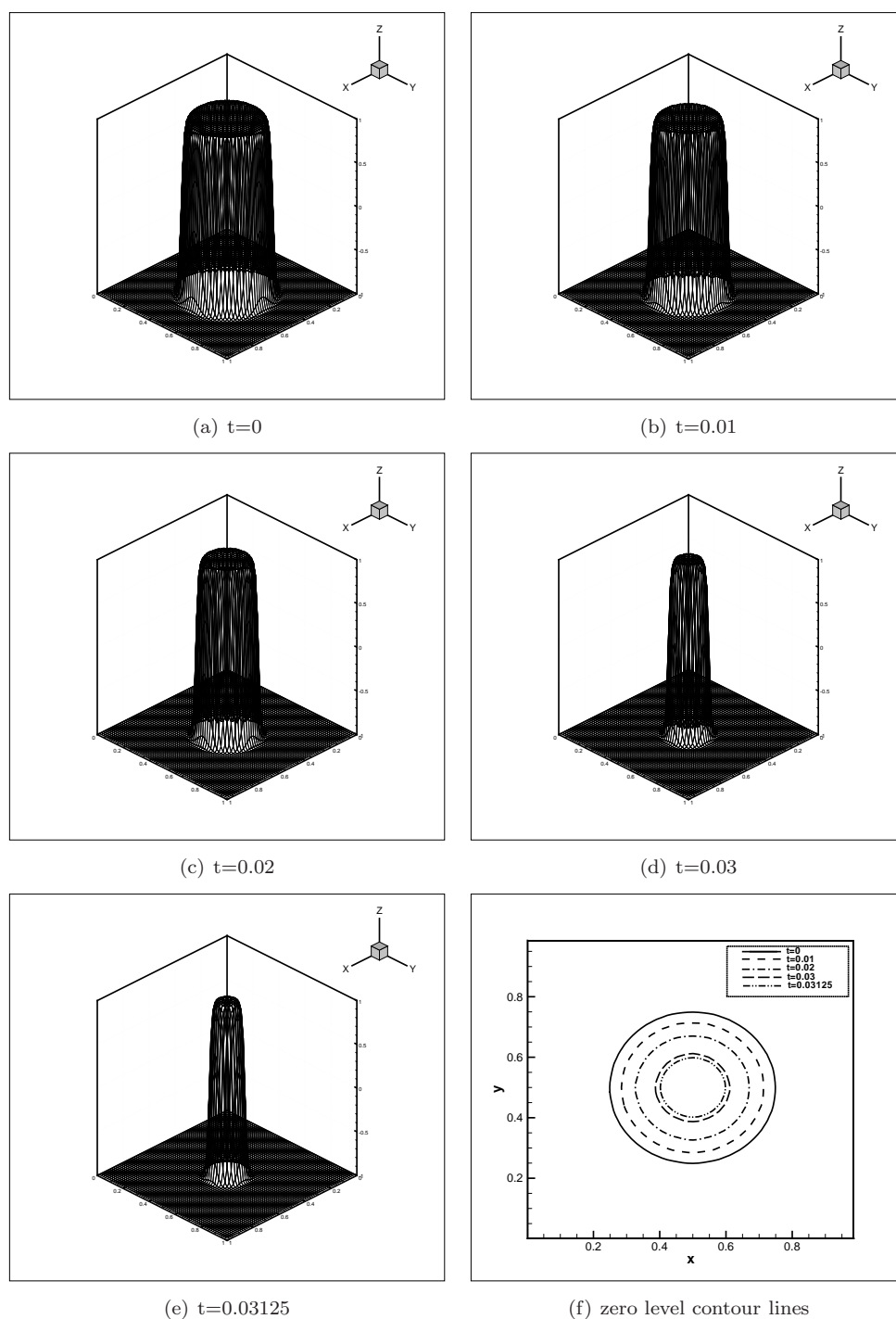


Fig. 4.3. (a)-(e) show the evolution of the initial condition in Example 4.5. (f) shows the zero level contour lines of (a)-(e).

with Neumann boundary conditions in $\Omega = [0, 1] \times [0, 1]$ and initial condition

$$u(x, y, 0) = \tanh \left(\frac{0.25 - \sqrt{(x - 0.5)^2 + (y - 0.5)^2}}{\sqrt{2}\varepsilon} \right), \quad (4.6)$$

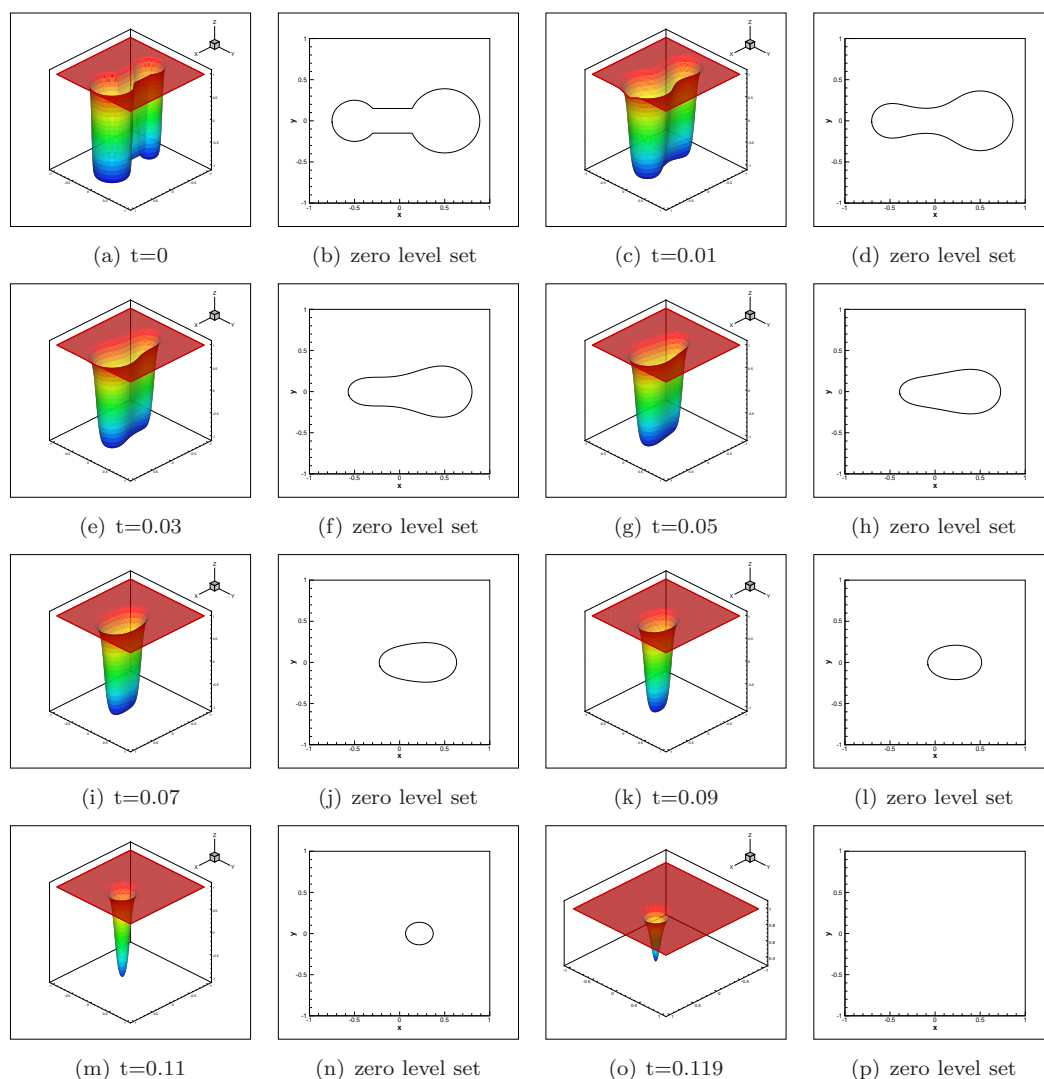


Fig. 4.4. The evolution of the initial condition and the zero level contour lines in Example 4.6.

where $\varepsilon = 0.01$. Fig. 4.3 shows the evolution of the initial condition and the zero level contour lines. We clearly see that the circle shrinks as theoretically predicted, which agrees with the numerical calculations performed by Choi *et al.* [7].

Example 4.6. We consider the Allen-Cahn equation

$$u_t - \Delta u + \frac{1}{\varepsilon^2} f(u) = 0 \quad (4.7)$$

with Neumann boundary conditions and the following initial condition

$$u(x, y, 0) = \begin{cases} \tanh\left(\frac{3}{\varepsilon}((x - 0.5)^2 + y^2 - (0.39)^2)\right), & \text{if } x > 0.14, \\ \tanh\left(\frac{3}{\varepsilon}(y^2 - (0.15)^2)\right), & \text{if } -0.3 \leq x \leq 0.14, \\ \tanh\left(\frac{3}{\varepsilon}((x + 0.5)^2 + y^2 - (0.25)^2)\right), & \text{if } x < -0.3, \end{cases} \quad (4.8)$$

where $\varepsilon = 0.05$. The computation domain is $\Omega = [-1, 1] \times [-1, 1]$. Fig. 4.4 shows snapshots of

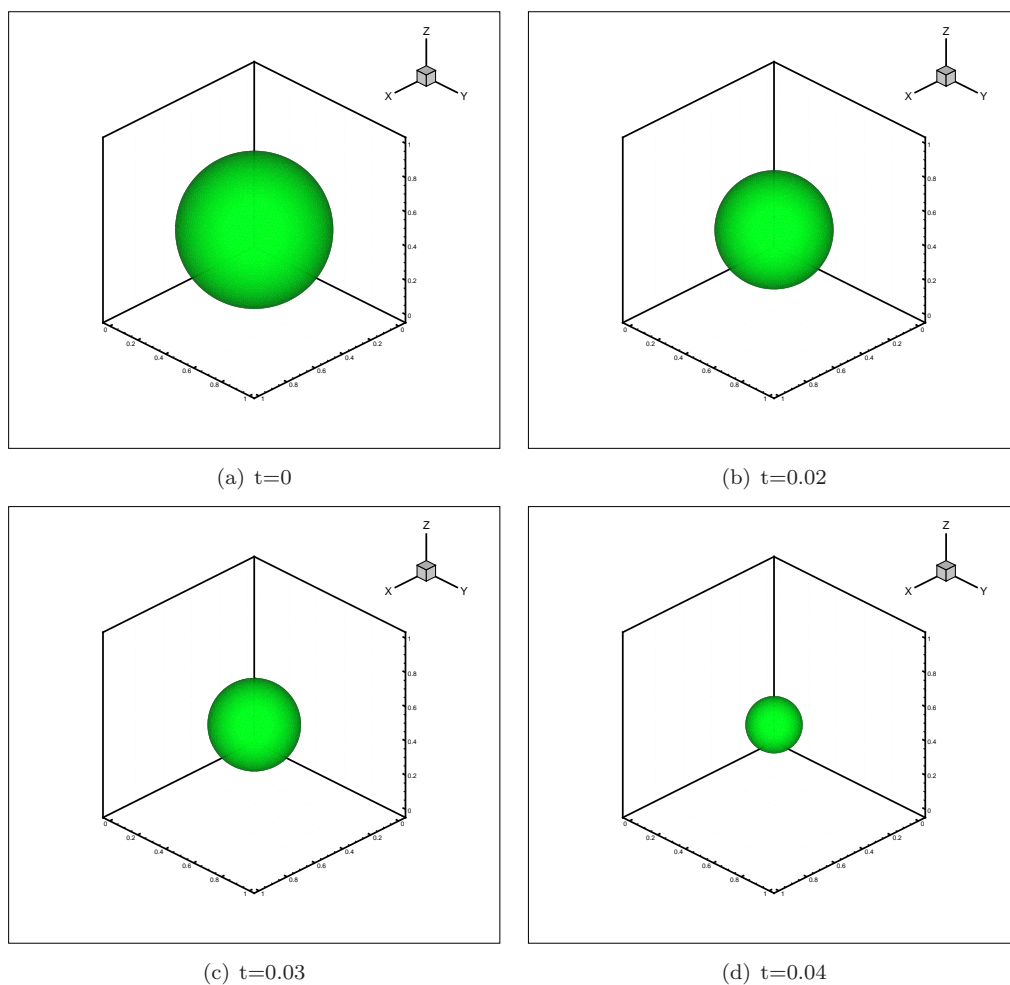


Fig. 4.5. The zero isosurface of the solution at different time for Example 4.7.

the solution and its zero level set of the Allen-Cahn equation. The numerical results compare very well with the numerical calculations performed by Feng *et al.* [15].

Example 4.7. We consider the equation

$$u_t - \Delta u + \frac{1}{\varepsilon^2} f(u) = 0 \quad (4.9)$$

with Neumann boundary conditions in $\Omega = [0, 1] \times [0, 1] \times [0, 1]$ and initial condition

$$u(x, y, z, 0) = \tanh \left(\frac{0.4 - \sqrt{(x-0.5)^2 + (y-0.5)^2 + (z-0.5)^2}}{\sqrt{2}\varepsilon} \right), \quad (4.10)$$

where $\varepsilon = 0.02$. Fig. 4.5 shows snapshots of the zero isosurface of the solution in three-dimensional space. The times are shown below each figure. The numerical results agree with the numerical calculations in [21].

5. Concluding Remarks

In this paper, we have developed an LDG method for the Allen-Cahn equation and proved the energy stability. We have presented the optimal error analysis in L^2 norm for the LDG method. By employing a technical dual argument, we have demonstrated that we obtain an accuracy of $\mathcal{O}(h^{2k+1})$ in the negative-order norm for all space dimension $d \leq 3$ and polynomial degree $k \geq 1$. Furthermore, in addition to these theoretical results, we demonstrate numerically that we can indeed improve the LDG solution from $\mathcal{O}(h^{k+1})$ to $\mathcal{O}(h^{2k+1})$ with the accuracy enhancement post-processing technique.

We presented an unconditionally energy stable convex splitting scheme for the Allen-Cahn equation, but the scheme is only first order accurate in time. To achieve higher order temporal accuracy, the semi-implicit SDC method was employed. The equations at the implicit time level are nonlinear and we employed an efficient nonlinear multigrid solver to solve the equations. Numerical examples for one-dimensional, two-dimensional and three-dimensional cases were given to illustrate the accuracy and capability of the LDG method coupled with the semi-implicit SDC time marching method.

Acknowledgements. Research supported by NSFC grant No. 11371342.

References

- [1] S. Allen and J.W. Cahn, A microscopic theory for antiphase boundary motion and its application to antiphase domain coarsening, *Acta Metall.*, **27** (1979), 1084-1095.
- [2] S. Bartels and R. Müller, Quasi-optimal and robust a posteriori error estimates in $L^\infty(L^2)$ for the approximation of Allen-Cahn equations past singularities, *Math. Comp.*, **80** (2011), 761-780.
- [3] A. Brandt, Multigrid techniques: 1984 guide with applications to fluid dynamics. GMD-Studien [GMD Studies], 85. Gesellschaft für Mathematik und Datenverarbeitung mbH, St. Augustin, 1984.
- [4] Susanne C. Brenner and L. Ridgway Scott, The mathematical theory of finite element methods, Springer.
- [5] L.Q. Chen, Phase-field models for microstructure evolution, *Ann. Rev. Mater. Res.*, **32** (2002), 113-140.
- [6] X.F. Chen, C.M. Elliott, A. Gardiner and J.J. Zhao, Convergence of numerical solutions to the Allen-Cahn equation, *Appl. Anal.*, **69** (1998), 47-56.
- [7] J.W. Choi, H.G. Lee, D. Jeong and J. Kim, An unconditionally gradient stable numerical method for solving the Allen-Cahn equation, *Physica A*, **388** (2009), 1791-1803.
- [8] P. Ciarlet, The finite element method for elliptic problem, North Holland, 1975.
- [9] B. Cockburn and C.-W. Shu, The local discontinuous Galerkin method for time-dependent convection-diffusion systems, *SIAM J. Numer. Anal.*, **35** (1998), 2440-2463.
- [10] B. Cockburn, G. Kanschat, I. Perugia and D. schötzau, Superconvergence of the local discontinuous Galerkin method for elliptic problems on cartesian grids, *SIAM J. Numer. Anal.*, **39** (2001), 264-285.
- [11] B. Dong and C.-W. Shu, Analysis of a local discontinuous Galerkin method for fourth-order time-dependent problems. *SIAM J. Numer. Anal.*, **47** (2009), 3240-3268.
- [12] A. Dutt, L. Greengard and V. Rokhlin, Spectral deferred correction methods for ordinary differential equations, *BIT*, **40** (2000), 241-266.
- [13] X.B. Feng, Y.K. Li, Analysis of interior penalty discontinuous Galerkin methods for the Allen-Cahn equation and the mean curvature flow, preprint, arXiv:1310.7504.
- [14] X.B. Feng and A. Prohl, Numerical analysis of the Allen-Cahn equation and approximation for mean curvature flows, *Numer. Math.*, **94** (2003), 33-65.

- [15] X.B. Feng and H.J. Wu, A posteriori error estimates and an adaptive finite element method for the Allen-Cahn equation and the mean curvature flow, *J. Sci. Comput.*, **24** (2005), 121-146.
- [16] X. Feng, H. Song, T. Tang, and J. Yang, Nonlinear stability of the implicit-explicit methods for the Allen-Cahn equation, *Inverse Problems and Imaging (A special issue in honor of Tony Chan's 60th birthday)* **7** (2013), 679-695.
- [17] X. Feng, T. Tang, and J. Yang, Long time numerical simulations for phase-field problems using p-adaptive spectral deferred correction methods, *SIAM J. Sci. Comput.*, **37** (2015), A271-A294.
- [18] R. Guo and Y. Xu, Efficient solvers of discontinuous Galerkin discretization for the Cahn-Hilliard equations, *J. Sci. Comput.*, **58** (2014), 380-408.
- [19] L. Ji, Y. Xu and J.K. Ryan, Accuracy-enhancement of discontinuous Galerkin solutions for convection-diffusion equations in multiple-dimensions, *Math. Comp.*, **81** (2012), 1929-1950.
- [20] L. Ji, Y. Xu and J.K. Ryan, Negative-order norm estimates for nonlinear hyperbolic conservation laws, *J. Sci. Comput.*, **54** (2013), 531-548.
- [21] Y. Li, H.G. Lee, D. Jeong and J. Kim, An unconditionally stable hybrid numerical method for solving the Allen-Cahn equation, *Computers and Mathematics with Applications*, **60** (2010), 1591-1606.
- [22] H. Liu and J. Yan, A local discontinuous Galerkin method for the Korteweg-de Vries equation with boundary effect, *J. Comput. Phys.*, **215** (2006), 197-218.
- [23] M.L. Minion, Semi-implicit spectral deferred correction methods for ordinary differential equations, *Commun. Math. Sci.*, **1** (2003), 471-500.
- [24] W.H. Reed and T.R. Hill, Triangular mesh method for the neutron transport equation, Technical report LA-UR-73-479, Los Alamos Scientific Laboratory, Los Alamos, NM, 1973.
- [25] J. Shen and X. Yang, Numerical approximations of Allen-Cahn and Cahn-Hilliard equations, *iscret. Contin. Dyn. Syst.*, **28** (2010), 1669-1691.
- [26] A.A. Wheeler, W.J. Boettinger and G.B. McFadden, Phase-field model for isothermal phase transitions in binary alloys, *Phys. Rev.*, A **45** (1992), 7424-7439.
- [27] Y. Xia, Y. Xu and C.-W. Shu, Local discontinuous Galerkin methods for the Cahn-Hilliard type equations, *J. Comput. Phys.*, **227** (2007), 472-491.
- [28] Y. Xia, Y. Xu and C.-W. Shu, Efficient time discretization for local discontinuous Galerkin methods, *Discrete Contin. Dyn. Syst. Ser. B*, **8** (2007), 677-693.
- [29] Y. Xia, Y. Xu and C.-W. Shu, Application of the local discontinuous Galerkin method for the Allen-Cahn/Cahn-Hilliard system, *Commun. Comput. Phys.*, **5** (2009), 821-835.
- [30] Y. Xu and C.-W. Shu, Local discontinuous Galerkin methods for two classes of two dimensional nonlinear wave equations, *Physica D*, **208** (2005), 21-58.
- [31] Y. Xu and C.-W. Shu, Local discontinuous Galerkin methods for high-order time-dependent partial differential equations, *Communications in Computational Physics*, **7** (2010), 1-46.
- [32] J. Yan and C.-W. Shu, A local discontinuous Galerkin method for KdV type equations, *SIAM J. Numer. Anal.*, **40** (2002), 769-791.
- [33] X.F. Yang, Error analysis of stabilized semi-implicit method of Allen-Cahn equation, *Discrete Contin. Dyn. Syst.-Ser. B*, **11** (2009), 1057-1070.
- [34] J. Zhang and Q. Du, Numerical studies of discrete approximations to the Allen-Cahn equation in the sharp interface limit, *SIAM J. Sci. Comput.*, **31** (2009), 3042-3063.